Nano Lett. 2019, 19, 8, 5496–5505
https://doi.org/10.1021/acs.nanolett.9b02035

Origin of Nanoscale Friction Contrast between Supported Graphene, MoS_2, and a Graphene/MoS_2 Heterostructure

Mohammad R. Vazirisereshk[1‡], Han Ye[2‡], Zhijiang Ye[3], Alberto Otero-de-la-Roza[4], Mengqiang Zhao[5], Zhaoli Gao[5], A. T. Charlie Johnson[5], Erin R. Johnson[6], Robert W. Carpick[2] and Ashlie Martini[1]**

[1] Department of Mechanical Engineering, University of California, Merced, CA 95343, USA

[2] Department of Mechanical Engineering and Applied Mechanics, University of Pennsylvania, Philadelphia, PA 19104, USA

[3] Department of Mechanical and Manufacturing, Miami University, Oxford, OH 45056, USA

[4] Departamento de Química Física y Analítica, Facultad de Química, Universidad de Oviedo, 33006 Oviedo, Spain

[5] Department of Physics and Astronomy, University of Pennsylvania, Philadelphia, PA 19104, USA

[6] Department of Chemistry, Dalhousie University, Halifax, NS B3H 4R2, Canada

Nano Lett. 2019, 19, 8, 5496–5505
https://doi.org/10.1021/acs.nanolett.9b02035

ABSTRACT: Ultra-low friction can be achieved with 2D materials, particularly graphene and MoS_2. The nanotribological properties of these different 2D materials have been measured in previous atomic force microscope (AFM) experiments sequentially, precluding immediate and direct comparison of their frictional behavior. Here, friction is characterized at the nanoscale using AFM experiments with the same tip sliding over graphene, MoS_2, and a graphene/MoS_2 heterostructure in a single measurement, repeated hundreds of times, and also measured with a slowly varying normal force. The same material systems are simulated using molecular dynamics (MD) and analyzed using density-functional theory (DFT) calculations. In both experiments and MD simulations, graphene consistently exhibits lower friction than the MoS_2 monolayer and the heterostructure. In some cases, friction on the heterostructure is lower than that on the MoS_2 monolayer. Quasi-static MD simulations and DFT calculations show that the origin of the friction contrast is the difference in energy barriers for a tip sliding across each of the three surfaces.

KEYWORDS: nanoscale friction, graphene vs. MoS_2, heterostructure, atomic force microscope, molecular dynamics, density-functional theory

Introduction

2D materials offer unique and intriguing possibilities for structural and mechanical applications thanks to their extreme mechanical properties, including large in-plane stiffness and low bending rigidity[1]. Further, their weak interlayer van der Waals interactions enable easy lamellar shear and intrinsically low friction and adhesion[2]. These materials thus have a unique combination of properties that enable them to exhibit ultra-low friction[2] and wear[3-6]. These features make 2D materials attractive as ultrathin solid-lubricant coatings and as additives for

liquid lubricants[2, 7-11]. For such applications, two of the most promising and frequently researched 2D materials are graphene and MoS_2[12].

Graphene's ability to suppress wear is attributed in part to its mechanical strength; its in-plane elastic stiffness is equivalent to a Young's modulus on the order of 1 TPa[13, 14]. Additionally, graphene has been shown to be impermeable with respect to different liquids[15] and gases[14], an important feature for corrosion/oxidation-resistant coatings. Graphene and graphite also exhibit ultra-low friction, as measured between an atomic force microscope (AFM) tip and a graphene or graphite substrate[7, 11, 16], or at graphene-graphene and graphite-graphite interfaces[17-19]. Such studies have explored the dependence of friction on the number of graphene layers, chemical modification, environmental/operating conditions, and commensurability. These have revealed that friction decreases with increasing numbers of graphene layers[7] and that this layer dependence is affected by a variety of factors, including out-of-plane stiffness[7] and the structure of the interface[20-22], as well as graphene-substrate adhesion[23, 24]. Graphene properties can be tuned with chemical modification, e.g., fluorination[25-27], hydrogenation[25], and oxidation[25]. These modifications lead to significant friction enhancement[26, 27], attributed to increased corrugation of the potential energy surface[26] as well as an increase in the atomic-scale roughness[28]. Graphene and graphite are also sensitive to environmental and operating conditions: friction varies with humidity nonmonotonically[29, 30], increases with decreasing temperature[31, 32], and increases with increasing speed[32, 33]. Lastly, the orientation of graphene relative to the scan direction of an AFM tip or of adjacent graphene sheets has a significant effect on friction[34]. The lowest friction possible is achieved with incommensurate structures, leading to the observation of superlubricity[35-37] for graphene sliding on graphene/graphite[18, 38] and on gold[39].

Like graphene, MoS_2 has anti-wear properties attributed in part to high effective in-plane Young's modulus (0.33 TPa in the case of freely suspended MoS_2[40]), and low intrinsic friction response. Friction of various materials sliding against MoS_2 has been studied using AFM, and it has been shown that mechanically-exfoliated MoS_2 exhibits layer-dependent friction similar to graphene[7]. Like with graphene and graphite, the tribological behavior of MoS_2 is also sensitive to the environment and testing conditions. In atmospheric conditions, adsorption of chemical compounds (H_2O or O_2) can disrupt the easy shearing properties of the lamellae, which increases friction[41]. Also, grain boundaries of polycrystalline MoS_2 can cause an oscillatory layer-dependent friction due to the absence and presence of polar grain boundaries with even and odd numbers of layers, respectively[42]. In addition to environmental factors, temperatures above 350K can lead to a substantial reduction in friction[43] and MoS_2 friction increases with increasing speed[44]. Lastly, MoS_2 frictional anisotropy has been measured with a periodicity of 60°[45-47], resulting from linearly aligned structures along the crystallographic axis of the honeycomb lattice structure[47]. This anisotropy has led to recent observations of superlubricity in MoS_2-MoS_2[48] and MoS_2-Sb[49] contacts.

Two recent studies have compared nanoscale friction on monolayer graphene and MoS_2 on SiO_2 substrates. In one study, a silver nanowire had lower friction when sliding on MoS_2 than for graphene[50]. In another study, friction measured with a Si AFM tip showed that the magnitude of friction force was lower on MoS_2, but friction increased with normal force less strongly on graphene[51]. In the former study the difference was attributed to adhesion, but the latter study suggested puckering as the origin of the friction contrast. Importantly, in these studies, friction was recorded on the two materials in separate measurements, i.e. the experiments were performed sequentially.

Previous research has shown that both graphene and MoS_2 can exhibit low friction and wear, but the behavior is sensitive to various conditions. In some cases, both materials exhibit similar trends (e.g., friction decreasing as temperature increases and orientation dependence) and in others different trends (e.g., environment dependence). Potentially, the properties of these two materials could be combined to leverage the unique features of both[52]. Integration of dissimilar 2D materials without the constraints of crystal lattice matching is possible due the weak van der Waals interlayer interactions of these materials[52]. Recently, heterostructures of MoS_2 and graphene have been developed, and their macroscale tribological behavior characterized. A ball-on-disk friction test showed that reduced graphene oxide (RGO)/MoS_2 heterostructures, used as oil additives and also dispersed in ethanol, decreased friction and wear compared to the lubricant with either RGO or MoS_2 alone[53-55]. This improvement was attributed to the lattice mismatch between RGO and MoS_2, as well as the contribution of adsorbed RGO/MoS_2 structures to passivate the sliding interfaces, thereby reducing the wear rate[55]. At atomic scale, an analytical study of the interlayer friction of a graphene/MoS_2 heterostructure revealed that the frictional energy for sliding graphene against MoS_2 was an order of magnitude smaller than that of homogenous bilayers[56]. This observation is in agreement with a combined Raman-based experimental/first-principles study of superlubricity at atomic scale in graphene/MoS_2 heterostructures that showed the heterostructure had a lower interlayer lateral force constant than homogeneous bilayers[57].

To summarize, studies to date have demonstrated that both graphene and MoS_2 can exhibit extremely low friction, and recent developments in heterostructure synthesis and fabrication may enable further improvements. However, all previous nanoscale friction measurements on graphene, MoS_2, and graphene/MoS_2 heterostructures were performed only on one of those

materials at a time, whereby the probe (e.g., an AFM tip) was slid against one material for some time period, then a different material. Therefore, the results could be affected by differences in parameters from experiment to experiment (e.g., tip size, morphology, and surface chemistry; sample preparation method and thus substrate surface chemistry; and environmental conditions, like humidity). The possibility of a significant change in the shape and/or the surface chemistry of the tip during an experiment is a particularly difficult challenge to address. While sequentially alternating from one sample to the other repeatedly is an effective approach, a more reliable approach is to directly compare the different substrate materials within a single AFM line scan. To accomplish this, here we produce graphene and MoS_2 monolayers on a single Si/SiO_2 substrate, establishing three surfaces: graphene on SiO_2, MoS_2 on SiO_2, and a heterostructure of MoS_2 on graphene on SiO_2, all accessible within the scan range of the AFM. Friction on these three surfaces is characterized using AFM and also by molecular dynamics (MD) simulations, complemented by density-functional theory (DFT) calculations of surface energies. The approach enables, for the first time, direct comparison between friction on graphene, MoS_2, and a graphene/MoS_2 heterostructure.

A Si/SiO_2 sample with supported graphene and MoS_2 monolayers and graphene/MoS_2 heterostructures all simultaneously present was prepared based on the method discussed in the methods section. Optical images of the samples are shown in Figures 1(a) and 1(b). Atomic scale friction was measured using an Asylum MFP-3D AFM in contact mode with a diamond like carbon (DLC) coated silicon tip. The measurements were performed at room temperature (~25°C) with a sliding speed of 4.30 μm/s in a dry nitrogen environment with RH ~3%. A schematic of the experiment is shown in Figure 1(c). The slow scan direction was disabled so the same line was continually scanned as the normal force was varied from 25 nN to almost -5 nN,

with the negative value resulting from sliding in the adhesive regime (Figure S1). The load range corresponds to estimated normal pressures from 3.62 to 1.90 GPa calculated using the continuum mechanics-based Derjaguin-Müller-Toporov (DMT)[58] model, which provides an approximation of the pressure in the absence of a specific model for 2D materials.

Complementary simulations were designed to capture the key aspects of the experiment and included the same three material systems. The model consisted of a graphene layer supported by a crystalline silicon (a-Si) substrate and an MoS_2 layer supported partially by the silicon substrate and partially by the graphene (see Figure 1(d)). The model tip was displaced laterally over the substrate with a constant speed of 2 m/s at normal loads ranging from 0.15 to 10 nN (corresponding to a pressure range from 5.2 to 9.3 GPa, calculated using the DMT model). Detailed information about the MD simulation setup can be found in the methods section. Density-functional theory (DFT) calculations were performed to model the corrugation of the potential energy surface (PES) for methane sliding over graphene and MoS_2 bilayers (Figure S2a,b) and to calculate adhesion energies. DFT calculation details are given in the methods section.

Results and Discussion.

The topography of a single region containing monolayer graphene, a heterostructure of MoS_2 on graphene, and monolayer MoS_2, measured by AFM is shown in Figure 2(a). While some residual contamination can be seen, the heights of the various regions can be determined with respect to the substrate. The height profiles in Figure 2(c) show that the thicknesses of the monolayers of graphene and MoS_2 are 0.26±0.12 nm and 0.76±0.16 nm, respectively (see section

3 of the supplementary information for additional Raman spectra analysis). The theoretical thickness of single-layer graphene and MoS_2 are reported to be 0.35[59] nm and 0.65[60] nm.

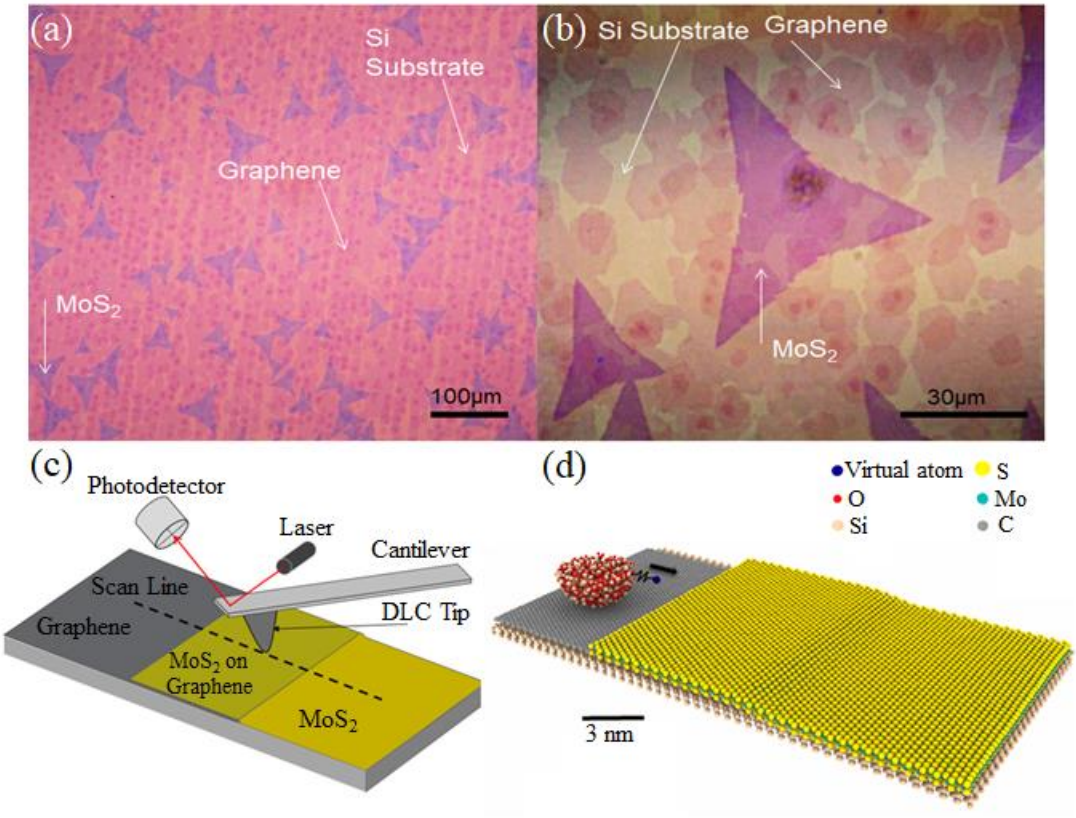

Figure 1. (a), (b) Optical microscope images of the samples containing graphene, the graphene/MoS_2 heterostructure, and MoS_2 on Si/SiO_2. (c) Schematic of the AFM experiment and (d) snapshot of the corresponding MD simulation.

Figure 2(b) shows the corresponding friction map, which indicates that friction is much higher on the SiO_2 substrate than for any of the 2D materials, as expected. The friction profile in Figure 2(c) enables direct comparison between the 2D materials and shows that friction on both monolayer MoS_2 and the heterostructure is larger than that on graphene. The same trend is seen in the simulations: friction is higher when the tip slides on MoS_2 as compared to graphene (see

Figure S4 for a representative friction trace from the MD simulation). Figure S4 also demonstrates the stick-slip friction observed in the simulations. Although we did not resolve atomic lattice stick-slip behavior in the AFM experiments, preliminary work to be published in the future shows that we can observe atomic stick-slip on this sample at the same speeds and compliance values. Thus, we are confident we are measuring static friction behavior.

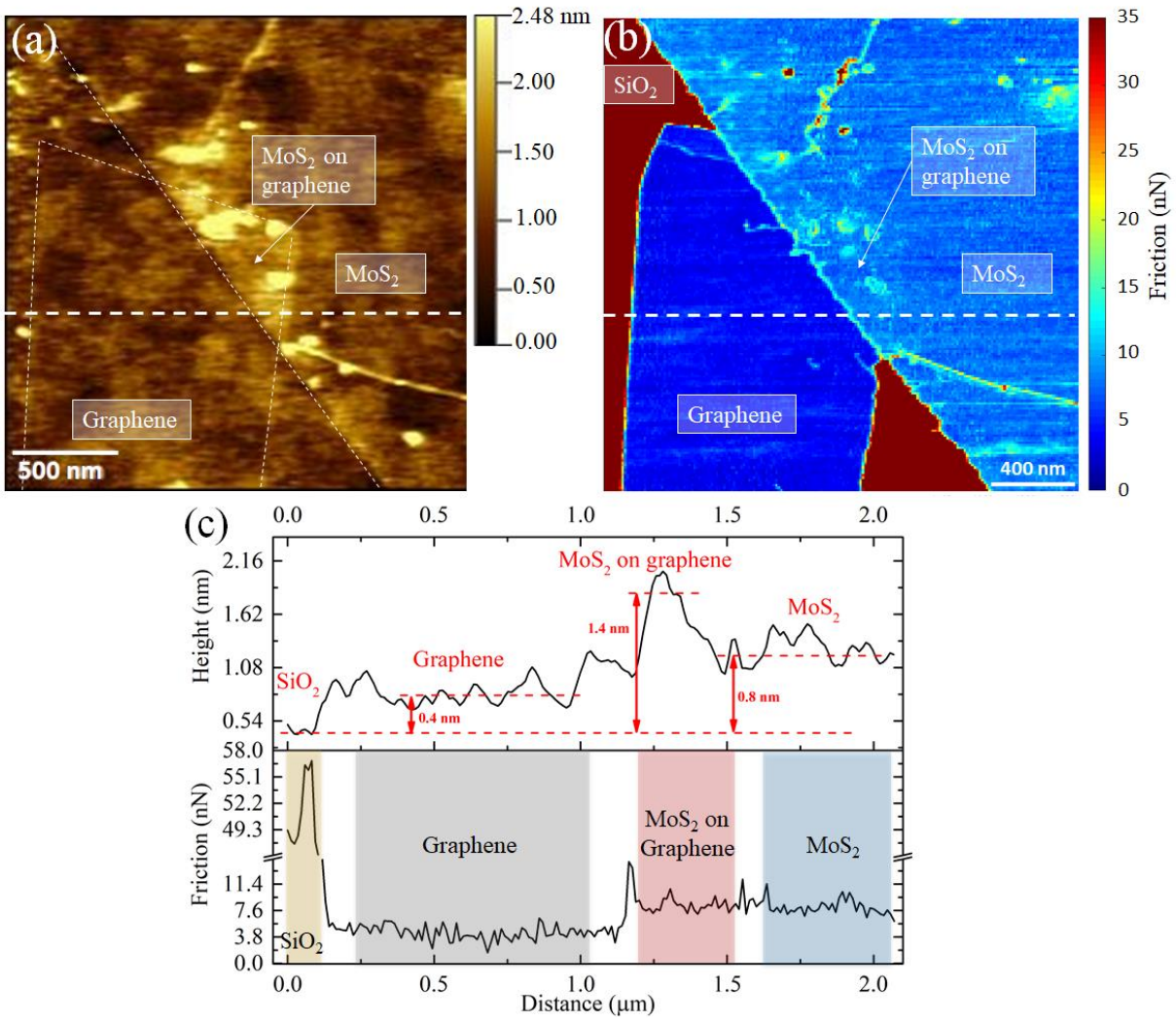

Figure 2. (a) AFM topographic image of graphene, MoS_2, and a graphene/MoS_2 heterostructure on a Si/SiO2 substrate obtained using contact mode AFM, and (b) friction map corresponding to the topographic image. (c) Height and friction profiles corresponding to the white dashed line in

(a) and (b) that indicate graphene and MoS_2 are monolayers, and show a clear friction contrast between MoS_2 and graphene. The AFM images in this Figure are taken at 12.29 nN load and 22.54 μm/s scanning speed. Some inhomogeneities are seen, which are attributed to remnant contamination from the polymethyl methacrylate (PMMA)-based transfer process and/or from adventitious carbon due to atmospheric exposure.

The load-dependence of friction for sliding on the three surfaces from experiment and simulation is shown in Figure 3. In both experiment (Figure 3(a)) and simulation (Figure 3(b)), the friction force on monolayer graphene is significantly lower than on either monolayer MoS_2 or the graphene/MoS_2 heterostructure (see Figure S5 for the topography corresponding to the friction data in Figure 3, and Figure S6 for another experimental dataset). At some loads, there is also higher friction force for MoS_2 on SiO_2 as compared to MoS_2 on graphene. This difference is only statistically significant in the simulations at a load of 3 nN, and it is only observed in ca. 14% of the experimental measurements (with at least 10% friction difference).

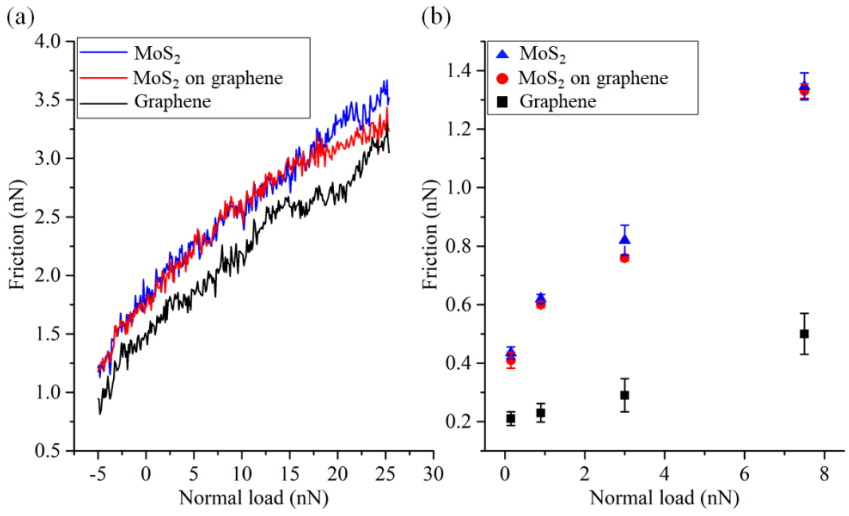

Figure 3. Friction as a function of load from (a) AFM and (b) MD. Friction on monolayer graphene is lower than on either monolayer MoS_2 or the graphene/MoS_2 heterostructure. The

error bars in (b) represent the standard deviation of the measured friction force in the MD simulation.

Comparing the simulations to experiments, the average friction force at each load in the experiments is higher than the average peak friction force at that same load in simulations. This is likely due to the larger tip used in the experiment (9.6 nm vs. 2 nm radius in simulations), which will result in a larger contact area and, in turn, greater friction[61]. Also, although the trends are the same, the difference between MoS_2 and graphene is greater in the simulations than in the experiments. This difference may be at least partially attributed to the presence of adsorbates in the experiments, which are not included in the model system. Such adsorbates are expected to increase friction by the same amount on both MoS_2 and graphene, such that the relative difference between MoS_2 and graphene is reduced in the experiments.

Several mechanisms of nanoscale static friction[2] might explain the friction contrast between the graphene and the two MoS_2 surfaces, and each of these is evaluated here. First, friction can be affected by thermal activation via the contribution of thermal energy to overcome local energy barriers and enable slip[62]. However, the main factors affecting this friction mechanism are speed and temperature, which are the same for all three surfaces. The relative crystallographic orientation of the graphene and MoS_2 with respect to sliding direction can also affect the atomic scale friction in both experiments and simulation[2]. However, the experimental data shown in Figure 2 and Figure S5 were measured for samples having different orientations relative to the sliding direction, yet the same friction trend was obtained from both orientations in AFM, as well as in the MD simulations.

Static friction can also be enhanced when material removal occurs, i.e. wear. The possibility of tip wear during the test was evaluated by comparing pre- and post-measurement transmission electron microscope (TEM) images of the tip and variation of friction and adhesion over time. TEM images (Figure S7) showed that some change in the tip shape occurred during the test. However, analysis of the lateral force calibration images and contact mechanics models[63, 64] suggested that the observed wear likely occurred during lateral force calibration, such that the tip was unchanged during the friction measurements (see Section 7 of the supplementary information). This is further confirmed by the fact that the difference between the pre- and post-test adhesion on each surface was less than the error associated with the adhesion measurement. Finally, capturing friction measurements of the three regions repeatedly in the same image, line after line, eliminated the possibility that friction differences seen were attributed to tip changes. The friction was consistent (with <3% standard error) at each normal load throughout the experiment. Moreover, no wear was observed in the MD simulations. Therefore, material removal cannot explain the friction contrast between the different materials.

Friction can also be affected by elastic deformation, i.e. the out-of-plane deformation causes bending and stretching in the lattices and acts to enhance static friction[7, 65]. A direct experimental evaluation of the local deformation is not possible without sub-angstrom resolution indentation[66]. However, MD simulations provide detailed atomistic information of the buried contact between the AFM tip and substrate. As shown in Figure S8, the out-of-plane deformation of the 2D materials increases with load, but there is no statistically significant difference between the deformation of the three surfaces. We also investigated the possibility of the friction contrast being due to the difference in the surface roughness, which has been shown to enhance friction due to better interlocking of the atoms at the interface[20]. However, there is no consistent

difference in the root-mean-square (RMS) roughness of the three surfaces observed in either AFM or MD (Figures S9 and S10), which indicates that roughness is not a dominant mechanism determining friction contrast.

Another important factor determining friction for nanoscale contacts is adhesion[67]. This effect can be measured in both experiments and simulations as the maximum adhesive force experienced as the tip is pulled away from the surface. The pull-off force is shown in Figure S11. Although the magnitude of the adhesive force differs between experiment and simulation, which we attribute primarily to the different tip sizes, the work of adhesion values calculated using the DMT model are comparable (Figure S12). Comparing graphene and MoS_2, adhesion is larger for graphene as measured from both experiment and MD simulation, in agreement with previous measurements[51, 68]. This trend is also corroborated by binding energies calculated from DFT (table S1). The breakdown of these energies shows that the base-functional energy has a positive contribution to the adhesion, indicating no favorable electrostatics and significant non-bonded repulsion. All of the adhesion energy originates from the dispersion term and, although the dispersion contribution to the binding is higher for MoS_2 than graphene, the total adhesion is weaker. This can be attributed to the larger atomic size of S, which would lead to greater repulsion for a similar methane-surface distance. DFT calculations were not performed for the heterostructure because the periodic boundary conditions would strain either the MoS_2 or graphene due to their misaligned lattice constants. Regardless, the adhesion difference between graphene and MoS_2 in DFT, MD, and experiments is opposite to the trend observed for friction, so adhesion cannot explain the friction contrast.

The remaining factor is the tip-sample interaction energy. In the classical Prandtl-Tomlinson (PT)[62, 69] model, at zero temperature, static friction is directly proportional to the height of the

energy barrier that the tip must overcome to slip forward, i.e., the corrugation of the interfacial potential energy surface[70]. To quantify this for the three surfaces, we used quasi-static MD simulations in which an oxygen atom was used to raster scan over each surface and calculated the minimum energy at each lateral position. Figure 4 shows the complete potential energy surface (PES) for each region. The maximum energy barrier is much smaller for graphene than either MoS_2 or the heterostructure (~16 meV smaller). Further, the heterostructure energy barrier is slightly smaller (2.4 meV smaller) than that of the MoS_2. Since these simulations were based on an empirical potential, the energy barriers for MoS_2 and graphene were also calculated using DFT. The methane molecule (in two different configurations as shown in Figures S2(c) and S2(d)) was translated diagonally over the three surfaces. DFT results (Figure 4(d) and Figure S13) for both methane configurations are consistent with the empirical model in terms of the relative differences between energy barriers for the graphene and MoS_2 surfaces.

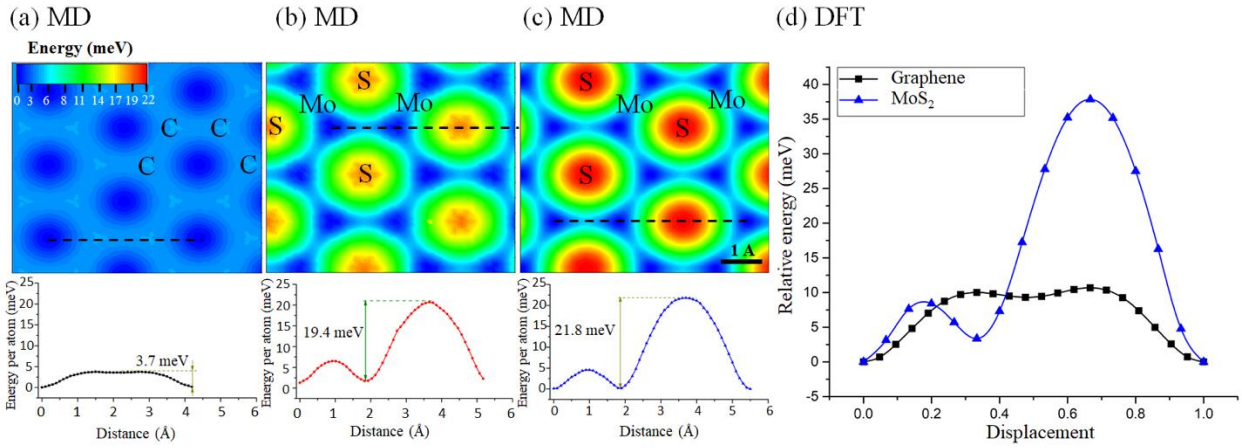

Figure 4. (a) Potential energy surfaces (PES) for the three surfaces calculated using quasi-static simulations for (a) graphene, (b) the graphene/MoS_2 heterostructure, and (c) MoS_2. A cross-sectional energy profile corresponding to the dashed line on the contour plot is shown below each contour. (d) Relative energy barrier calculated using DFT for translation of methane along

the long diagonal of the hexagonal unit cell of graphene and MoS_2 bilayers. The x-axis represents the fractional displacement across the unit cell. Symbols correspond to the ab initio data; lines are guides for the eyes only.

Importantly, the energy trends found from empirical simulations of an oxygen atom and DFT calculations of methane are consistent with the friction observed in the MD simulations of an SiO_2 tip and experiments with a DLC tip. In the case of an atom sliding over these barriers, one can expect the atom to slide over the saddle points with lower barriers leading to almost identical friction between these materials. However, during the AFM experiment or MD simulation, the tip apex consists of an ensemble of atoms in the buried contact some of which will necessarily move over energy barrier maxima. This suggests that energetic barriers to sliding explain the friction contrast between the three materials. Interestingly, we observe slightly higher adhesion between the tip and graphene compared with the adhesion between the tip and MoS_2. However, the relative difference of the adhesion to these two surfaces in our AFM experiments and MD simulations (see table S3) is small with respect to the relative friction contrast observed. Moreover, increased adhesion will increase contact area, according to most contact mechanics models, and it has been seen to increase the interfacial shear strength[71]. In both cases, this would increase interfacial friction. We thus attribute the increased friction to the increased energy barrier, with adhesion making little difference.

Although the energy barriers were obtained from static calculations at 0 K, the barrier heights are expected to determine friction contrast at finite temperatures and speeds. According to the thermal PT model, the approximate relationship between friction (F), temperature (T), and speed (v) is $F = F_C - \left|\beta k_B T ln(\frac{v_c}{v})\right|^{\frac{2}{3}}$, where F_C is the maximum friction at 0K, β is a parameter

determined by the shape of the potential, k_B is Boltzmann's constant, and v_c is the critical speed, above which friction starts to become speed-independent[61]. The magnitude of F_C is directly proportional to barrier height. The second term in the equation increases sub-linearly with barrier height due to the dependence of β and v_c on F_c, thus the net effect of increasing barrier height will be larger friction at any temperature and speed.

Next, we consider why the energy barriers are different for these three surfaces. Comparing graphene and MoS_2 energy barriers from DFT, the difference is due entirely to the dispersion contributions (see table S2). At the minimum-energy configurations, there is greater dispersion binding of the model tip to MoS_2, which stems from the sulphur anions in MoS_2 being more polarizable than carbon atoms in graphene. Coupled with the atomic corrugation of the MoS_2 surface, which reduces the dispersion binding at the maximum-energy configuration, this leads to higher sliding barriers for MoS_2 relative to graphene[72]. The finding that friction contrast between MoS_2 and graphene is due to sliding energy barriers also may explain the difference between our results and those from a previous study that showed friction is lower on MoS_2 than graphene[50]. Friction in that study was measured with a silver nanowire, and the nature of the interaction of silver with graphene or MoS_2 is likely different from those we observe with non-metallic, non-reactive materials.

DFT calculations were not performed for the heterostructure as it would require introducing unphysical lattice strain as mentioned earlier. However, the energy barrier difference between the MoS_2 and the heterostructure could be explained by the quasi-static MD simulations. Analysis of the relative contributions of the layers to the energy barrier, which consists entirely of van der Waals interactions in the MD simulation, showed that the contribution of the upper MoS_2 layer was the same for the monolayer and the heterostructure (18.5±0.2 meV). However, the graphene

layer in the heterostructure contributes 1.0 meV to the energy barrier, while the silicon substrate beneath the MoS_2 monolayer contributes 3.1 meV. Therefore, the heterostructure has a slightly lower energy barrier because the graphene contribution is less than that of the silicon. This difference is small, which explains why the friction in dynamic simulations and in experiments, which is determined both by potential energy and thermally-driven hopping over energy barriers, is only sometimes observed to be smaller for the heterostructure. This interpretation is limited by the fact that the relative twist orientation of the MoS_2 and graphene layers in the heterostructure was not known; further study is required to determine how strongly friction depends on this twist angle.

Conclusions.

In this study, we report a direct comparison of nanoscale static friction between a diamondlike carbon AFM tip and monolayer graphene, monolayer MoS_2, and a graphene/MoS_2 heterostructure, all supported on an Si/SiO_2 substrate. Both experiments and MD simulations showed that MoS_2 has higher friction than graphene across a wide range of normal loads. The friction measured for sliding on the graphene/MoS_2 heterostructure was comparable to, but occasionally lower than, that for monolayer MoS_2. The origin of the friction contrast between sliding on graphene vs. MoS_2 was shown not to be scanning speed, tip change, roughness, adhesion, or other environmental factors. Instead, quasi-static simulations with an empirical potential, and with DFT calculations, demonstrated that the origin of the friction contrast is the difference in energy barriers to sliding on the two surfaces. The energy barrier difference between MoS_2 and graphene is due to the higher dispersion contribution to the sliding barrier for MoS_2, due to the higher polarizability of S atoms compared to C. The quasi-static MD simulations showed that the difference in friction between sliding on MoS_2 and sliding on the

heterostructure results from the dispersion contribution of the underlying material (graphene *vs.* silicon) to the energy barrier. These findings have implications for continued development and application of heterostructures with unique and potentially tunable properties.

Methods.

Sample preparation: The substrate was a die cut from a Si(100) wafer with 285 nm of thermally-grown SiO_2. Discontinuous graphene flakes were grown on a copper foil using atmospheric-pressure chemical vapor deposition (CVD) based on an established method[73]. Briefly, Cu foils (Alfa Aesar Item #46365) were cleaned with 5.4% HNO_3 for 40 seconds and two DI water baths for 2 minutes. The Cu foils were then loaded into the furnace (Lindberg blue M, TF55035). The furnace was ramped to 1050 ºC at a rate of 60 ºC/min in a flow of 500 sccm Ar + 30 sccm H_2. After 5 minutes annealing, graphene flakes were grown by introducing 2.5 sccm CH_4 (1% in Ar) for 15 minutes. After growth, the reactor was rapidly cooled to room temperature in a flow of 10 sccm H_2 and 1000 sccm Ar. Discontinuous graphene flakes were then transferred onto the Si/SiO_2 substrate using the bubble transfer method[74]. During the bubble transfer procedure, a layer of polymethyl methacrylate (PMMA) was spin-coated on the graphene on the copper substrate at 3000 rpm for 60 s. The spin-coated sample was baked at 100 ºC for 2 min and then immersed in a 0.05 mol/L NaOH aqueous solution with applied 20 V voltage between the copper foil and the solution. PMMA-supported graphene was delaminated from the Cu foil by hydrogen gas bubbles formed at the graphene-Cu surface. The floating PMMA/graphene film was washed with distilled water (resistivity of 18.2 MΩ cm), and then carefully placed in contact with the Si/SiO_2 die. After drying, the PMMA was removed by treating in acetone overnight, washed with isopropyl alcohol (IPA), and then annealed in vacuum (4×10^{-4} Torr) at 600° C for 150 minutes to remove the PMMA[75], leaving the graphene/Si/SiO_2

sample. The monolayer MoS_2 was CVD-grown on another Si/SiO_2 substrate[76] and transferred onto the graphene/Si/SiO_2 sample. The transfer involved spin coating the MoS_2 with PMMA and etching the SiO_2 interface by the 1 M KOH method[77]. The floating PMMA/MoS_2 film was washed with distilled water twice and placed on the top of the graphene/Si/SiO_2 sample. The PMMA was removed by treating in acetone for 2 hours, washed with IPA, and annealed in vacuum at 600° C for 150 minutes to remove the PMMA. Optical images (Olympus BX51 Microscope with Olympus C-5050Z camera) of the samples are shown in Figures 1(a) and 1(b). Raman spectroscopy (NT-MDT NTEGRA) shown in Figure S3 confirms that monolayer graphene and monolayer MoS_2 were present on the sample. The possibility of oxidization of the materials during sample preparation was analyzed and determined to be negligible, as discussed in section 13 of supplementary information.

Friction force measurements: Friction was measured using an Asylum MFP-3D AFM (DLC) coated silicon tip (BudgetSensors ContDLC) with a radius of curvature of 9.6±0.4 nm estimated from TEM images (JEOL F200 TEM, Figure S7). The normal and lateral cantilever force constant calibrations (k_{normal} = 0.087 N/m, $k_{lateral}$ = 28.3 N/m) were performed via the thermal tune method[78] and the wedge method[79], respectively. Friction was measured as a function of applied normal load, starting at a maximum load and then reducing the load by 0.1 nN per scan line until the tip pulled off the sample. This was accomplished using a program provided by Asylum Research Technical Support to ramp the normal force set point after each friction loop with the feedback still engaged, thus reducing wear and any changes in load due to changes in local surface height. The scan location was carefully chosen so that the AFM tip scanned across the three surfaces of interest: (1) monolayer graphene on the SiO_2 substrate, (2) monolayer MoS_2 on monolayer graphene on SiO_2, and (3) monolayer MoS_2 on SiO_2.

MD simulation: The MD model consisted of a graphene layer and an MoS_2 layer supported partially by the silicon substrate and partially by the graphene (see Figure 1(d)). To incorporate the compliance of the AFM cantilever, we coupled the model tip (2 nm radius) to an interaction-free particle (virtual atom in Figure 1(d)) via a harmonic spring (stiffness of 1.6 N/m) representing the cantilever [61]. The substrate and the atoms at one end of the graphene and MoS_2 sheets were fixed in place and the tip was treated as a rigid body. The potentials used for interactions within each material were AIREBO for graphene[80] and REBO[81] for MoS_2. A Lennard–Jones 6–12 potential was employed to describe all interactions between the materials (parameters in table S4). The simulations were performed at 300 K in NVT (constant number of atoms, volume and temperature) ensemble using a Nosé–Hoover thermostat[82] (excluding the direction of sliding from the temperature calculation), consistent with previous simulations of atomic friction[83-85]. The simulations were performed with the LAMMPS[86] code and the atomic configurations were imaged using OVITO[87]. During a simulation, the tip was first brought in contact with the substrate and the entire system was relaxed for 0.7 ns, at which point the vertical position of the tip varied less than 0.05 Å. Then, friction tests were performed by displacing the virtual atom laterally with a constant speed of 2 m/s at normal loads ranging from 0.15 to 10 nN. The sliding speed in simulations was orders of magnitude larger than that in the experiments due to the fs-scale time step in the simulations. While the speed gap between simulations and experiments can be addressed using simulations with parallelization in time[88], that approach was not viable here since the large model size required the available computational resources be used for spatial parallelization. Further, it has been shown that the same friction trends can be obtained using AFM and MD with very different sliding speeds[16, 29]. We therefore used this approach here. During each sliding simulation, the lateral force on the virtual atom was recorded.

The lateral force exhibited stick-slip behavior in all cases and friction was calculated as the average of the peak lateral forces, i.e. static friction[89].

DFT calculations: In order to model the corrugation of the potential energy surfaces (PES) for a methane sliding over graphene and MoS_2 bilayers (Figure S2a,b), DFT calculation were performed. All calculations used the B86bPBE[90, 91] functional with the exchange-hole dipole moment dispersion model (XDM)[92, 93], implemented in the Quantum ESPRESSO package[94]. The XDM damping function coefficients have the canonical values for the B86bPBE functional[95] (a_1=0.6512, a_2=1.4633). The projector-augmented wave (PAW) method[96] with datasets from the Quantum ESPRESSO pslibrary[97] were used. The cutoff energies were 80 Ry for the wavefunctions and 800 Ry for the density. A uniform k-point sampling of 5x5x1 was used for graphene and 2x2x1 for MoS_2. The atomic positions and in-plane lattice constants of graphene and MoS_2 bilayers were relaxed, while the surface-normal dimension of the unit cell was kept fixed, providing 30 Å of vacuum between each surface and its periodic image. The energy and force convergence thresholds were 10^{-6} Ry and 10^{-5} Ry/bohr, respectively, and these same values were used for all geometry relaxations in this work.

To generate the sliding PES, a single methane molecule was used to represent the AFM tip, as in our previous work[98]. While this does not at all match the dimensions of the tips used in the MD simulations and experiments, the DFT calculations are limited to model tips of molecular dimensions. The resulting barriers should represent an upper bound to the corrugation of the PES, since incommensurability resulting from larger tips will tend to reduce this corrugation. Adsorption of the model methane tip on the surface was considered in two different configurations, shown in Figure S4(c,d). The methane was adsorbed on the equilibrium geometries of the graphene or MoS_2 bilayers, using 3x3 supercells to prevent methane-methane

self-interactions. The horizontal coordinates of the methane molecule on the surface and the atomic positions of the graphene and MoS_2 layers were kept fixed, while the vertical position of methane molecule was allowed to relax. A 6x6 uniform sampling of methane positions was used to explore the two-dimensional sliding PES. In addition, calculations of methane sliding along the long diagonal of the hexagonal unit cell (Figure S4) were carried out for both bilayers. These sliding-energy barriers have been shown to control friction in the low-temperature limit, according to the PT model and scale well with experimental nanoscale friction measurements[26, 70].

ASSOCIATED CONTENT

Supplementary information accompanies this paper.

AUTHOR INFORMATION

Corresponding Author

To whom correspondence should be addressed. E-mail: amartini@ucmerced.edu and carpick@seas.upenn.edu

Author Contributions

‡These authors contributed equally to this work.

HY carried out the experiments, advised by RWC. MRV performed the MD simulations, advised by AM. MZ and ZG prepared the sample, advised by ATCJ. AOR and ERJ performed the DFT calculations. ZY contributed to the preliminary design of the MD simulation setup. The manuscript was written through contributions of all authors.

Funding Sources

This work was funded by the National Science Foundation, awards CMMI-1762384 and CMMI-1761874.

ACKNOWLEDGMENT

MZ and ATCJ acknowledge support from the National Science Foundation EFRI-2DARE program, grant number ENG-1542879. AOR thanks the Spanish Ministerio de Economıa y Competitividad (MINECO) for a Ramón y Cajal fellowship (RyC-2016-20301). ERJ thanks the Natural Sciences and Engineering Research Council of Canada for financial support. This work used the Extreme Science and Engineering Discovery Environment (XSEDE), which is supported by National Science Foundation grant number ACI-1548562. The authors acknowledge the University of Pennsylvania's Singh Center for Nanotechnology, an NNCI member supported by NSF Grant ECCS-1542153, technical support and discussion from K. Hasz, Dr. H. Khare, Dr. M. Brukman, Dr. J.B. Dr. McClimon, J. Hilbert, K. Tian, Dr. J. Lefever, Dr. C. Naylor, and Dr. Z. Milne.

ABBREVIATIONS

AFM, atomic force microscope; MD, molecular dynamics; DFT, density-functional theory; DLC, diamond like carbon; RH, relative humidity; DMT, Derjaguin-Müller-Toporov; RMS, root-mean-square; PT, Prandtl-Tomlinson; PES, potential energy surface; CVD, chemical vapor

deposition; PMMA, polymethyl methacrylate; IPA, isopropyl alcohol; TEM, transmission electron microscope.

REFERENCES

(1) Androulidakis, C.; Zhang, K.; Robertson, M.; Tawfik, S., Tailoring the mechanical properties of 2D materials and heterostructures. *2D Mater.* **2018,** *5* (3), 032005.

(2) Berman, D.; Erdemir, A.; Sumant, A. V., Approaches for Achieving Superlubricity in Two-Dimensional Materials. *ACS Nano* **2018,** *12* (3), 2122-2137.

(3) Klemenz, A.; Pastewka, L.; Balakrishna, S. G.; Caron, A.; Bennewitz, R.; Moseler, M., Atomic Scale Mechanisms of Friction Reduction and Wear Protection by Graphene. *Nano Lett.* **2014,** *14* (12), 7145-7152.

(4) Vasić, B.; Matković, A.; Ralević, U.; Belić, M.; Gajić, R., Nanoscale wear of graphene and wear protection by graphene. *Carbon* **2017,** *120*, 137-144.

(5) Berman, D.; Erdemir, A.; Sumant, A. V., Reduced wear and friction enabled by graphene layers on sliding steel surfaces in dry nitrogen. *Carbon* **2013,** *59*, 167-175.

(6) Mungse, H. P.; Khatri, O. P., Chemically Functionalized Reduced Graphene Oxide as a Novel Material for Reduction of Friction and Wear. *J. Phys. Chem. C* **2014,** *118* (26), 14394-14402.

(7) Lee, C.; Li, Q.; Kalb, W.; Liu, X.-Z.; Berger, H.; Carpick, R. W.; Hone, J., Frictional Characteristics of Atomically Thin Sheets. *Science* **2010,** *328* (5974), 76.

(8) Kim, K.-S.; Lee, H.-J.; Lee, C.; Lee, S.-K.; Jang, H.; Ahn, J.-H.; Kim, J.-H.; Lee, H.-J., Chemical Vapor Deposition-Grown Graphene: The Thinnest Solid Lubricant. *ACS Nano* **2011,** *5* (6), 5107-5114.

(9) Shin, Y. J.; Stromberg, R.; Nay, R.; Huang, H.; Wee, A. T. S.; Yang, H.; Bhatia, C. S., Frictional characteristics of exfoliated and epitaxial graphene. *Carbon* **2011,** *49* (12), 4070-4073.

(10) Berman, D.; Deshmukh, S. A.; Sankaranarayanan, S. K. R. S.; Erdemir, A.; Sumant, A. V., Macroscale superlubricity enabled by graphene nanoscroll formation. *Science* **2015,** *348* (6239), 1118.

(11) Egberts, P.; Han, G. H.; Liu, X. Z.; Johnson, A. T. C.; Carpick, R. W., Frictional Behavior of Atomically Thin Sheets: Hexagonal-Shaped Graphene Islands Grown on Copper by Chemical Vapor Deposition. *ACS Nano* **2014,** *8* (5), 5010-5021.

(12) Akinwande, D.; Brennan, C. J.; Bunch, J. S.; Egberts, P.; Felts, J. R.; Gao, H.; Huang, R.; Kim, J.-S.; Li, T.; Li, Y.; Liechti, K. M.; Lu, N.; Park, H. S.; Reed, E. J.; Wang, P.; Yakobson, B. I.; Zhang, T.; Zhang, Y.-W.; Zhou, Y.; Zhu, Y., A review on mechanics and mechanical properties of 2D materials-Graphene and beyond. *Extrem. Mech. Lett.* **2017,** *13*, 42-77.

(13) Lee, G.-H.; Cooper, R. C.; An, S. J.; Lee, S.; van der Zande, A.; Petrone, N.; Hammerberg, A. G.; Lee, C.; Crawford, B.; Oliver, W.; Kysar, J. W.; Hone, J., High-Strength Chemical-Vapor–Deposited Graphene and Grain Boundaries. *Science* **2013,** *340* (6136), 1073.

(14) Bunch, J. S.; Verbridge, S. S.; Alden, J. S.; van der Zande, A. M.; Parpia, J. M.; Craighead, H. G.; McEuen, P. L., Impermeable Atomic Membranes from Graphene Sheets. *Nano Lett.* **2008,** *8* (8), 2458-2462.

(15) He, K. T.; Wood, J. D.; Doidge, G. P.; Pop, E.; Lyding, J. W., Scanning Tunneling Microscopy Study and Nanomanipulation of Graphene-Coated Water on Mica. *Nano Lett.* **2012,** *12* (6), 2665-2672.

(16) Egberts, P.; Ye, Z.; Liu, X. Z.; Dong, Y.; Martini, A.; Carpick, R. W., Environmental dependence of atomic-scale friction at graphite surface steps. *Phys. Rev. B* **2013,** *88* (3), 035409.

(17) Liu, Z.; Yang, J.; Grey, F.; Liu, J. Z.; Liu, Y.; Wang, Y.; Yang, Y.; Cheng, Y.; Zheng, Q., Observation of Microscale Superlubricity in Graphite. *Phys. Rev. Lett.* **2012,** *108* (20), 205503.

(18) Feng, X.; Kwon, S.; Park, J. Y.; Salmeron, M., Superlubric Sliding of Graphene Nanoflakes on Graphene. *ACS Nano* **2013,** *7* (2), 1718-1724.

(19) Sinclair, R. C.; Suter, J. L.; Coveney, P. V., Graphene–Graphene Interactions: Friction, Superlubricity, and Exfoliation. *Adv. Mater* **2018,** *30* (13), 1705791.

(20) Ye, Z.; Balkanci, A.; Martini, A.; Baykara, M. Z., Effect of roughness on the layer-dependent friction of few-layer graphene. *Phys. Rev. B* **2017,** *96* (11), 115401.

(21) Li, S.; Li, Q.; Carpick, R. W.; Gumbsch, P.; Liu, X. Z.; Ding, X.; Sun, J.; Li, J., The evolving quality of frictional contact with graphene. *Nature* **2016,** *539*, 541.

(22) Smolyanitsky, A.; Killgore, J. P.; Tewary, V. K., Effect of elastic deformation on frictional properties of few-layer graphene. *Phys. Rev. B* **2012,** *85* (3), 035412.

(23) Li, Q.; Lee, C.; Carpick, R. W.; Hone, J., Substrate effect on thickness-dependent friction on graphene. *Phys. Stat. Solidi B* **2010,** *247* (11-12), 2909-2914.

(24) Cho, D.-H.; Wang, L.; Kim, J.-S.; Lee, G.-H.; Kim, E. S.; Lee, S.; Lee, S. Y.; Hone, J.; Lee, C., Effect of surface morphology on friction of graphene on various substrates. *Nanoscale* **2013,** *5* (7), 3063-3069.

(25) Ko, J.-H.; Kwon, S.; Byun, I.-S.; Choi, J. S.; Park, B. H.; Kim, Y.-H.; Park, J. Y., Nanotribological Properties of Fluorinated, Hydrogenated, and Oxidized Graphenes. *Tribol. Lett.* **2013,** *50* (2), 137-144.

(26) Li, Q.; Liu, X.-Z.; Kim, S.-P.; Shenoy, V. B.; Sheehan, P. E.; Robinson, J. T.; Carpick, R. W., Fluorination of Graphene Enhances Friction Due to Increased Corrugation. *Nano Lett.* **2014,** *14* (9), 5212-5217.

(27) Kwon, S.; Ko, J.-H.; Jeon, K.-J.; Kim, Y.-H.; Park, J. Y., Enhanced Nanoscale Friction on Fluorinated Graphene. *Nano Lett.* **2012,** *12* (12), 6043-6048.

(28) Dong, Y.; Wu, X.; Martini, A., Atomic roughness enhanced friction on hydrogenated graphene. *Nanotechnology* **2013,** *24* (37), 375701.

(29) Hasz, K.; Ye, Z.; Martini, A.; Carpick, R. W., Experiments and simulations of the humidity dependence of friction between nanoasperities and graphite: The role of interfacial contact quality. *Phys. Rev. Mater.* **2018**, *2*, 126001

(30) Arif, T.; Colas, G.; Filleter, T., Effect of Humidity and Water Intercalation on the Tribological Behavior of Graphene and Graphene Oxide. *ACS Appl. Mater. Interfaces* **2018,** *10* (26), 22537-22544.

(31) Zhang, Y.; Dong, M.; Gueye, B.; Ni, Z.; Wang, Y.; Chen, Y., Temperature effects on the friction characteristics of graphene. *Appl. Phys. Lett.* **2015,** *107* (1), 011601.

(32) Jansen, L.; Hölscher, H.; Fuchs, H.; Schirmeisen, A., Temperature Dependence of Atomic-Scale Stick-Slip Friction. *Phys. Rev. Lett.* **2010,** *104* (25), 256101.

(33) Peng, Y.; Wang, Z.; Li, C., Study of nanotribological properties of multilayer graphene by calibrated atomic force microscopy. *Nanotechnology* **2014,** *25* (30), 305701.

(34) Choi, J. S.; Kim, J.-S.; Byun, I.-S.; Lee, D. H.; Lee, M. J.; Park, B. H.; Lee, C.; Yoon, D.; Cheong, H.; Lee, K. H.; Son, Y.-W.; Park, J. Y.; Salmeron, M., Friction Anisotropy–Driven Domain Imaging on Exfoliated Monolayer Graphene. *Science* **2011,** *333* (6042), 607.

(35) Baykara, M. Z.; Vazirisereshk, M. R.; Martini, A., Emerging superlubricity: A review of the state of the art and perspectives on future research. *Appl. Phys. Rev.* **2018,** *5* (4), 041102.

(36) Leven, I.; Krepel, D.; Shemesh, O.; Hod, O., Robust Superlubricity in Graphene/h-BN Heterojunctions. *J. Phys. Chem. C* **2013,** *4* (1), 115-120.

(37) Dienwiebel, M.; Verhoeven, G. S.; Pradeep, N.; Frenken, J. W. M.; Heimberg, J. A.; Zandbergen, H. W., Superlubricity of Graphite. *Phys. Rev. Lett.* **2004,** *92* (12), 126101.

(38) Liu, Y.; Song, A.; Xu, Z.; Zong, R.; Zhang, J.; Yang, W.; Wang, R.; Hu, Y.; Luo, J.; Ma, T., Interlayer Friction and Superlubricity in Single-Crystalline Contact Enabled by Two-Dimensional Flake-Wrapped Atomic Force Microscope Tips. *ACS Nano* **2018,** *12* (8), 7638-7646.

(39) Kawai, S.; Benassi, A.; Gnecco, E.; Söde, H.; Pawlak, R.; Feng, X.; Müllen, K.; Passerone, D.; Pignedoli, C. A.; Ruffieux, P.; Fasel, R.; Meyer, E., Superlubricity of graphene nanoribbons on gold surfaces. *Science* **2016,** *351* (6276), 957.

(40) Castellanos-Gomez, A.; Poot, M.; Steele, G. A.; van der Zant, H. S. J.; Agraït, N.; Rubio-Bollinger, G., Elastic Properties of Freely Suspended MoS_2 Nanosheets. *Adv. Mater* **2012,** *24* (6), 772-775.

(41) Zhao, X.; Perry, S. S., The Role of Water in Modifying Friction within MoS2 Sliding Interfaces. *ACS Appl. Mater. Interfaces* **2010,** *2* (5), 1444-1448.

(42) Lavini, F.; Calò, A.; Gao, Y.; Albisetti, E.; Li, T.-D.; Cao, T.; Li, G.; Cao, L.; Aruta, C.; Riedo, E., Friction and work function oscillatory behavior for an even and odd number of layers in polycrystalline MoS_2. *Nanoscale* **2018,** *10* (17), 8304-8312.

(43) Zhao, X.; Phillpot, S. R.; Sawyer, W. G.; Sinnott, S. B.; Perry, S. S., Transition from Thermal to Athermal Friction under Cryogenic Conditions. *Phys. Rev. Lett.* **2009,** *102* (18), 186102.

(44) Sheehan, P. E.; Lieber, C. M., Friction between van der Waals Solids during Lattice Directed Sliding. *Nano Lett.* **2017,** *17* (7), 4116-4121.

(45) Onodera, T.; Morita, Y.; Nagumo, R.; Miura, R.; Suzuki, A.; Tsuboi, H.; Hatakeyama, N.; Endou, A.; Takaba, H.; Dassenoy, F.; Minfray, C.; Joly-Pottuz, L.; Kubo, M.; Martin, J.-M.; Miyamoto, A., A Computational Chemistry Study on Friction of h-MoS_2. Part II. Friction Anisotropy. *J. Phys. Chem. B* **2010,** *114* (48), 15832-15838.

(46) Sheehan, P. E.; Lieber, C. M., Nanotribology and Nanofabrication of MoO_3 Structures by Atomic Force Microscopy. *Science* **1996,** *272* (5265), 1158.

(47) Lee, J. H.; Lee, S.; Jeon, J. H.; Oh, D. Y.; Shin, M.; Lee, M. J.; Shinde, S.; Ahn, J.-H.; Roh, C. J.; Lee, J. S.; Park, B. H., Universality of strain-induced anisotropic friction domains on 2D materials. *NPG Asia Mater.* **2018**, *10*, 1069–1075

(48) Li, H.; Wang, J.; Gao, S.; Chen, Q.; Peng, L.; Liu, K.; Wei, X., Superlubricity between MoS_2 Monolayers. *Adv. Mater* **2017,** *29* (27), 1701474.

(49) Dietzel, D.; Brndiar, J.; Štich, I.; Schirmeisen, A., Limitations of Structural Superlubricity: Chemical Bonds versus Contact Size. *ACS Nano* **2017,** *11* (8), 7642-7647.

(50) Zeng, X.; Peng, Y.; Lang, H.; Yu, K., Probing the difference in friction performance between graphene and MoS_2 by manipulating the silver nanowires. *J. Mater. Sci.* **2019,** *54* (1), 540-551.

(51) Khac, B.-C. T.; Chung, K.-H., Quantitative Assessment of Friction Characteristics of Single-Layer MoS_2 and Graphene Using Atomic Force Microscopy. *J. Nanosci. Nanotechnol.* **2016,** *16*(5), 4428-33

(52) Liu, Y.; Weiss, N. O.; Duan, X.; Cheng, H.-C.; Huang, Y.; Duan, X., Van der Waals heterostructures and devices. *Nat. Rev. Mater.* **2016,** *1*, 16042.

(53) Song, W.; Yan, J.; Ji, H., Fabrication of GNS/MoS_2 composite with different morphology and its tribological performance as a lubricant additive. *Appl. Surf. Sci.* **2019,** *469*, 226-235.

(54) Hou, K.; Wang, J.; Yang, Z.; Ma, L.; Wang, Z.; Yang, S., One-pot synthesis of reduced graphene oxide/molybdenum disulfide heterostructures with intrinsic incommensurateness for enhanced lubricating properties. *Carbon* **2017,** *115*, 83-94.

(55) Chen, J.; Xia, Y.; Yang, J.; Chen, B., Fabrication of monolayer MoS_2/rGO hybrids with excellent tribological performances through a surfactant-assisted hydrothermal route. *Appl. Phys. A* **2018,** *124* (6), 430.

(56) Jiang, J.-W.; Park, H. S., A Gaussian treatment for the friction issue of Lennard-Jones potential in layered materials: Application to friction between graphene, MoS_2, and black phosphorus. *J. Appl. Phys.* **2015,** *117* (12), 124304.

(57) Wang, L.; Zhou, X.; Ma, T.; Liu, D.; Gao, L.; Li, X.; Zhang, J.; Hu, Y.; Wang, H.; Dai, Y.; Luo, J., Superlubricity of a graphene/MoS_2 heterostructure: a combined experimental and DFT study. *Nanoscale* **2017,** *9* (30), 10846-10853.

(58) Jacobs, T.; Mate, C. M.; Turner, K.; Carpick, R. W., Understanding the tip-sample contact: An overview of contact mechanics at the nanoscale. In *Scanning probe microscopy for industrial applications: nanomechanical characterization*; Yablon, D. G., Ed.; Wiley Publishing, **2013**; pp. 15–48.

(59) Gupta, A.; Chen, G.; Joshi, P.; Tadigadapa, S.; Eklund, Raman Scattering from High-Frequency Phonons in Supported n-Graphene Layer Films. *Nano Lett.* **2006,** *6* (12), 2667-2673.

(60) Lee, Y.-H.; Zhang, X.-Q.; Zhang, W.; Chang, M.-T.; Lin, C.-T.; Chang, K.-D.; Yu, Y.-C.; Wang, J. T.-W.; Chang, C.-S.; Li, L.-J.; Lin, T.-W., Synthesis of Large-Area MoS_2 Atomic Layers with Chemical Vapor Deposition. *Adv. Mater* **2012,** *24* (17), 2320-2325.

(61) Dong, Y.; Vadakkepatt, A.; Martini, A., Analytical Models for Atomic Friction. *Tribol. Lett.* **2011,** *44* (3), 367.

(62) Prandtl, L., Ein Gedankenmodell zur kinetischen Theorie der festen Körper. *Z. Angew. Math. Mech.* **1928,** *8* (2), 85-106.

(63) Reedy, E. D., Contact mechanics for coated spheres that includes the transition from weak to strong adhesion. *J. Mater. Res.* **2007,** *22* (9), 2617-2622.

(64) Jacobs, T. D. B.; Ryan, K. E.; Keating, P. L.; Grierson, D. S.; Lefever, J. A.; Turner, K. T.; Harrison, J. A.; Carpick, R. W., The Effect of Atomic-Scale Roughness on the Adhesion of Nanoscale Asperities: A Combined Simulation and Experimental Investigation. *Tribol. Lett.* **2013,** *50* (1), 81-93.

(65) Deng, Z.; Smolyanitsky, A.; Li, Q.; Feng, X.-Q.; Cannara, R. J., Adhesion-dependent negative friction coefficient on chemically modified graphite at the nanoscale. *Nat. Mater.* **2012,** *11*, 1032.

(66) Gao, Y.; Kim, S.; Zhou, S.; Chiu, H.-C.; Nélias, D.; Berger, C.; de Heer, W.; Polloni, L.; Sordan, R.; Bongiorno, A.; Riedo, E., Elastic coupling between layers in two-dimensional materials. *Nat. Mater.* **2015,** *14*, 714.

(67) Waghmare, A. K.; Sahoo, P., Adhesive friction at the contact between rough surfaces using n-point asperity model. *Engineering Science and Technology, an International Journal* **2015,** *18* (3), 463-474.

(68) Li, P.; You, Z.; Cui, T., Molybdenum disulfide dc contact MEMS shunt switch. *J. Micromech. Microeng.* **2013,** *23* (4), 045026.

(69) Tomlinson, G. A., CVI. A molecular theory of friction. *Philos. Mag.* **1929,** *7* (46), 905-939.

(70) Socoliuc, A.; Bennewitz, R.; Gnecco, E.; Meyer, E., Transition from stick-slip to continuous sliding in atomic friction: entering a new regime of ultralow friction. *Phys. Rev. Lett.* **2004,** *92* (13), 134301.

(71) Carpick, R. W.; Agraït, N.; Ogletree, D. F.; Salmeron, M., Variation of the Interfacial Shear Strength and Adhesion of a Nanometer-Sized Contact. *Langmuir* **1996,** *12* (13), 3334-3340.

(72) Ye, Z.; Otero-de-la-Roza, A.; Johnson, E.; Martini, A., Oscillatory motion in layered materials: graphene, boron nitride, and molybdenum disulfide. *Nanotechnology* **2015,** *26* (16), 165701.

(73) Gao, Z.; Zhang, Q.; Naylor, C. H.; Kim, Y.; Abidi, I. H.; Ping, J.; Ducos, P.; Zauberman, J.; Zhao, M.-Q.; Rappe, A. M.; Luo, Z.; Ren, L.; Johnson, A. T. C., Crystalline Bilayer Graphene with Preferential Stacking from Ni–Cu Gradient Alloy. *ACS Nano* **2018,** *12* (3), 2275-2282.

(74) Lerner, M. B.; Matsunaga, F.; Han, G. H.; Hong, S. J.; Xi, J.; Crook, A.; Perez-Aguilar, J. M.; Park, Y. W.; Saven, J. G.; Liu, R.; Johnson, A. T. C., Scalable Production of Highly Sensitive Nanosensors Based on Graphene Functionalized with a Designed G Protein-Coupled Receptor. *Nano Lett.* **2014,** *14* (5), 2709-2714.

(75) Xie, W.; Weng, L.-T.; Ng, K. M.; Chan, C. K.; Chan, C.-M., Clean graphene surface through high temperature annealing. *Carbon* **2015,** *94*, 740-748.

(76) Naylor, C. H.; Kybert, N. J.; Schneier, C.; Xi, J.; Romero, G.; Saven, J. G.; Liu, R.; Johnson, A. T. C., Scalable Production of Molybdenum Disulfide Based Biosensors. *ACS Nano* **2016,** *10* (6), 6173-6179.

(77) Dumcenco, D.; Ovchinnikov, D.; Sanchez, O. L.; Gillet, P.; Alexander, D. T.; Lazar, S.; Radenovic, A.; Kis, A., Large-area MoS_2 grown using H_2S as the sulphur source. *2D Mater.* **2015,** *2* (4), 044005.

(78) Hutter, J. L.; Bechhoefer, J. Calibration of atomic-force microscope tips. *Rev. Sci. Instrum.* **1993**, 64, 1868– 1873.

(79) Ogletree, D.; Carpick, R. W.; Salmeron, M., Calibration of frictional forces in atomic force microscopy. *Rev. Sci. Instrum.* **1996,** *67* (9), 3298-3306.

(80) Stuart, S. J.; Tutein, A. B.; Harrison, J. A., A reactive potential for hydrocarbons with intermolecular interactions. *J. Chem. Phys.* **2000,** *112* (14), 6472-6486.

(81) Liang, T.; Phillpot, S. R.; Sinnott, S. B., Parametrization of a reactive many-body potential for Mo-S systems. *Phys. Rev. B* **2009,** *79* (24), 245110.

(82) Nosé, S., A unified formulation of the constant temperature molecular dynamics methods. *J. Chem. Phys.* **1984,** *81* (1), 511-519.

(83) Kobayashi, K.; Liang, Y.; Amano, K.-i.; Murata, S.; Matsuoka, T.; Takahashi, S.; Nishi, N.; Sakka, T., Molecular Dynamics Simulation of Atomic Force Microscopy at the Water–Muscovite Interface: Hydration Layer Structure and Force Analysis. *Langmuir* **2016,** *32* (15), 3608-3616.

(84) AlMotasem, A. T.; Bergström, J.; Gåård, A.; Krakhmalev, P.; Holleboom, L. J., Atomistic Insights on the Wear/Friction Behavior of Nanocrystalline Ferrite During Nanoscratching as Revealed by Molecular Dynamics. *Tribol. Lett.* **2017,** *65* (3), 101.

(85) Adams, H. L.; Garvey, M. T.; Ramasamy, U. S.; Ye, Z.; Martini, A.; Tysoe, W. T., Shear-Induced Mechanochemistry: Pushing Molecules Around. *J. Phys. Chem. C* **2015,** *119* (13), 7115-7123.

(86) Plimpton, S., Fast Parallel Algorithms for Short-Range Molecular Dynamics. *J. Comput. Phys.* **1995,** *117* (1), 1-19.

(87) Stukowski, A., Visualization and analysis of atomistic simulation data with OVITO–the Open Visualization Tool. *Modell. Simul. Mater. Sci. Eng.* **2010,** *18* (1), 015012.

(88) Liu, X.-Z.; Ye, Z.; Dong, Y.; Egberts, P.; Carpick, R. W.; Martini, A., Dynamics of Atomic Stick-Slip Friction Examined with Atomic Force Microscopy and Atomistic Simulations at Overlapping Speeds. *Phys. Rev. Lett.* **2015,** *114* (14), 146102.

(89) Carpick, R. W.; Salmeron, M., Scratching the Surface: Fundamental Investigations of Tribology with Atomic Force Microscopy. *Chemical Reviews* **1997,** *97* (4), 1163-1194.

(90) Becke, A., On the large-gradient behavior of the density functional exchange energy. *J. Chem. Phys.* **1986,** *85* (12), 7184-7187.

(91) Perdew, J. P.; Burke, K.; Ernzerhof, M., Generalized gradient approximation made simple. *Phys. Rev. Lett.* **1996,** *77* (18), 3865.

(92) Otero-de-la-Roza, A.; Johnson, E. R., Van der Waals interactions in solids using the exchange-hole dipole moment model. *J. Chem. Phys.* **2012,** *136* (17), 174109.

(93) Becke, A. D.; Johnson, E. R., Exchange-hole dipole moment and the dispersion interaction revisited. *J. Chem. Phys.* **2007,** *127* (15), 154108.

(94) Giannozzi, P.; Andreussi, O.; Brumme, T.; Bunau, O.; Nardelli, M. B.; Calandra, M.; Car, R.; Cavazzoni, C.; Ceresoli, D.; Cococcioni, M., Advanced capabilities for materials modelling with Quantum ESPRESSO. *J. Phys.: Condens. Matter* **2017,** *29* (46), 465901.

(95) http://schooner.chem.dal.ca/wiki/XDM.

(96) Blöchl, P. E., Projector augmented-wave method. *Phys. Rev. B* **1994,** *50* (24), 17953.

(97) https://dalcorso.github.io/pslibrary/.

(98) Ye, Z.; Otero-de-la-Roza, A.; Johnson, E. R.; Martini, A., Effect of tip shape on atomic-friction at graphite step edges. *Appl. Phys. Lett.* **2013,** *103* (8), 081601.